Available online at www.sciencedirect.com
SCIENCE DIRECT®
Journal of Sound and Vibration 285 (2005) 989–1014
JOURNAL OF SOUND AND VIBRATION
www.elsevier.com/locate/jsvi

Nonlinear shear-induced flexural vibrations of piezoceramic actuators: experiments and modeling

Sandeep Kumar Parashar*, Utz von Wagner, Peter Hagedorn

Department of Applied Mechanics, Darmstadt University of Technology, Hochschulstrasse 1, 64289 Darmstadt, Germany

Received 18 February 2004; received in revised form 19 July 2004; accepted 13 September 2004
Available online 7 December 2004

Abstract

In the piezoceramic actuators, the d_{15} effect is very attractive for the applications, as the shear piezoelectric coefficient d_{15} is higher than d_{31} and d_{33}. The potential use of the d_{15} effect of piezoceramics near the resonant frequency excitation, such as in ultrasonic motors and torsional actuators, has led to the close investigation of their behavior. At weak electric fields, the piezoceramics are usually described by linear constitutive relations. However, typical nonlinear effects such as softening behavior were observed in resonantly driven piezoceramic beams, which cannot be adequately defined by linear theories. In this paper, this nonlinear behavior has been modeled using higher-order cubic conservative and nonconservative terms in the constitutive equations. Series comprising orthogonal polynomial functions, generated using the Gram–Schmidt method, are used in the Rayleigh–Ritz method to formulate the linear eigenvalue problem. The linear eigenfunctions are used as shape functions to discretize the nonlinear equation of motion obtained by Hamilton's principle. The approximate solution of the nonlinear equation of motion is obtained using the perturbation method. Using this solution, nonlinear parameters are identified by comparing the theoretical and experimental results. The nonlinear effects and the modeling technique described herein may help in optimizing the existing applications and developing new applications based on the d_{15} effect.

*Corresponding author. Tel.: +49 6151 162486; fax: +49 6151 164125.
E-mail address: parashar@mechanik.tu-darmstadt.de (S.K. Parashar).

0022-460X/$ - see front matter © 2004 Elsevier Ltd. All rights reserved.
doi:10.1016/j.jsv.2004.09.012

1. Introduction

Fig. 1 shows a cantilever piezoceramic beam. The beam is polarized in the x_3-direction and the electric field is applied in the x_1-direction. The applied electric field induces flexural vibrations of the piezoceramic beam in the x_1x_3-plane due to d_{15}-effect. In the experiments the piezoceramic beam is excited near the first flexural resonance frequency at different excitation voltages. The tip displacement $u(h/2, l/2)$ is measured with the help of a laser vibrometer. The experimental results obtained by exciting a piezoceramic beam (PIC 255 manufactured by PI Ceramic at Lederhose, Germany) of the dimensions $18 \times 14 \times 8\,\text{mm}^3$ ($l \times b \times h$) are shown in Fig. 2. Typical nonlinear characteristics such as the dependence of the resonance frequency on the excitation voltage and a decrease in the normalized amplitude with increase in excitation voltage can be observed here.

In the present study, the nonlinear behavior of piezoceramics exhibited in the presence of weak electric field is studied. In contrast, the nonlinear behavior of piezoceramics in the presence of a strong electric field is a well-known phenomenon. Dielectric hysteresis and butterfly hysteresis are typical examples [1] of such behavior. Nonlinear behavior of the piezoceramics subjected to weak electric fields was investigated by Beige and Schmidt [2]. They observed typical nonlinear vibration behavior during an investigation of longitudinal vibrations of piezoceramics using d_{31} effect. Drögmöller and Gerlach [3] studied the jump phenomenon of current in piezoceramics, they attributed it to the nonlinear influence of the surrounding media. Jiang and Cao [4] investigated nonlinear properties of PZT piezoceramics. Mueller and Zhang [5] examined the nonlinear shear response of nonresonant excitation of PZT piezoceramics. Equivalent nonlinear effects as described by Beige and Schmidt were also found by Parashar and von Wagner [6,7] in the d_{31} effect, by von Wagner [8] in the d_{33} effect and by Parashar et al. [9,10] in d_{15} effect.

The use of the d_{15} effect is of particular interest as the shear piezoelectric coefficient is much higher than the other piezoelectric coefficients d_{31} and d_{33}. In the past few years, the interest in shear actuators has increased continuously. In particular, the applications of shear actuators to induce and control (smart structures) the flexural vibrations of beams and plates has been addressed quite frequently in the literature. Sun and Zhang [11] studied the effect of the actuator length and location on the actuation performance of an adaptive sandwich structure using the shear mode of piezoelectric material. Later [12], they presented formulation for an adaptive sandwich beam containing shear actuator by modeling the facing sheets as Euler–Bernoulli beam and central core as a Timoshenko beam. However, due to the complexity of the obtained electromechanical equations, the analysis was limited to a static case. This work was extended in Ref. [13] for the analysis of a sandwich plate based on the shear mode of piezoelectric material. The assumptions similar to the first-order shear deformation theory were used and Rayleigh–Ritz method was used to find the approximate solution. Benjeddou et al. [14] presented a unified beam

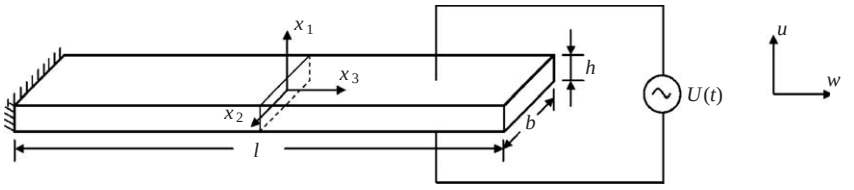

Fig. 1. x_3-axis polarized piezoceramic beam.

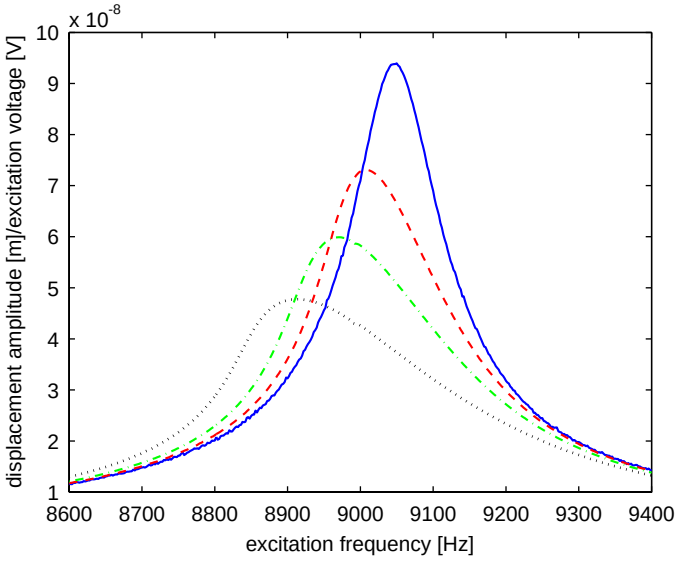

Fig. 2. Experimental normalized displacement response close to the first flexural resonance of piezoceramic cantilever beam at various excitation voltages (electric field strengths): — 2 V (0.25 V/mm); – – – 15 V (1.875 V/mm); – · – · – 30 V (3.75 V/mm); · · · · · · 60 V (7.5 V/mm).

finite element model for extension and shear piezoelectric actuation mechanisms. Trindade et al. [15] demonstrated that shear actuators can be more effective than thickness poled actuators for the control of bending vibrations. Aldraihem and Khdeir [16] investigated the feasibility of using shear-mode actuators in smart beams. They presented comparison of the analytical models based on first-order beam theory and higher-order beam theory. Vel and Batra [17] gave an exact solution for the static bending of a simply supported sandwich plate with an embedded piezoelectric shear actuator and compared the results with the one obtained from first-order shear deformation theory. In another effort [18], they provided an exact three-dimensional state space solution for the static cylindrical bending of simply supported laminated plates with embedded shear mode piezoelectric actuators.

Some new devices utilizing the d_{15} effect of the piezoceramics have also been reported in the literature. Glazounov et al. [19,20] introduced two novel devices, namely a torsional actuator and a torsional stepper motor based on piezoelectric d_{15} shear response. Kim and Kang [21] presented the design, test and improvement of the newly developed piezoelectric torsional actuator. A piezoelectric shear–shear mode ultrasonic motor based on the d_{15} effect is also proposed by Dong et al. [22].

Many of these applications, in particular ultrasonic motors, torsional actuators and some smart structures, discussed above utilize the piezoceramics near resonance frequency excitation. However, all of these published studies on shear actuators were restricted to a linear description of the piezoceramic behavior. The nonlinear effects observed in Fig. 2 are significant, and if ignored can cause an error up to 100% in the prediction of the amplitude and a large error in the prediction of the resonance frequencies. Hence, an efficient design of a device, utilizing the d_{15} effect, demands a detailed investigation of the observed nonlinear behavior. Parashar et al. [9]

investigated the nonlinear shear vibration of a free piezoceramic rectangular parallelepiped (with aspect ratio close to unity) at weak electric fields. They presented a simplified two-dimensional theory which takes into account only the shear stress in the structure. In the present paper, this work is extended to incorporate the normal stresses necessary for explaining the flexural vibrations of the piezoceramics. A detailed investigation of nonlinear shear-induced flexural vibration of piezoceramic beams, and a complete mathematical modeling of this nonlinear behavior, is believed to have not been reported in the literature before.

2. Linear modeling

In this section, first a reduced set of linear constitutive relations is obtained for the piezoceramic beam. Then, various energy expressions are obtained to be used in Hamilton's principle and in the Rayleigh–Ritz method. The field equations along with the boundary conditions are obtained using Hamilton's principle. As no closed-form solution is known for the obtained field equations, the Rayleigh–Ritz method is used to obtain eigenfunctions and eigenfrequencies of the system. The eigenfunctions thus obtained are used in the next section to discretize the nonlinear equation of motion in the Ritz method.

2.1. Linear constitutive equations

Under the assumption of plane stress (i.e. $T_2 = T_4 = T_6 = 0$) and neglecting the electric field E_2 in the transverse direction x_2, the linear constitutive equations for the piezoceramic beam can be written as [23]

$$T_1 = \overline{c}_{11}S_1 + \overline{c}_{13}S_3 - \overline{e}_{31}E_3, \tag{1}$$

$$T_3 = \overline{c}_{13}S_1 + \overline{c}_{33}S_3 - \overline{e}_{33}E_3, \tag{2}$$

$$T_5 = c_{44}^E S_5 - e_{15}E_1, \tag{3}$$

$$D_1 = \varepsilon_{11}^S E_1 + e_{15}S_5, \tag{4}$$

$$D_3 = \overline{\varepsilon}_{33}E_3 + \overline{e}_{31}S_1 + \overline{e}_{33}S_3 \tag{5}$$

with

$$\overline{c}_{11} = c_{11}^E - \left(c_{12}^{E^2}/c_{11}^E\right), \quad \overline{c}_{13} = c_{13}^E - \left(c_{12}^E c_{13}^E/c_{11}^E\right), \quad \overline{c}_{33} = c_{33}^E - \left(c_{13}^{E^2}/c_{11}^E\right),$$
$$\overline{e}_{31} = e_{31} - \left(c_{12}^E e_{31}/c_{11}^E\right), \quad \overline{e}_{33} = e_{33} - \left(c_{13}^E e_{31}/c_{11}^E\right), \quad \overline{\varepsilon}_{33} = \varepsilon_{33}^S + \left(e_{31}^2/c_{11}^E\right).$$

Here, S_p $(p = 1, 2, 3)$ are the normal strains, while S_p $(p = 4, 5, 6)$ are the shear strains. D_i are the dielectric displacements and E_i are the corresponding electric fields. c_{ij}^E are the stiffness coefficients, e_{ij} piezoelectric coefficients and $\varepsilon_{11}^S, \varepsilon_{33}^S$ denote the dielectric constants measured at constant strain. An overbar denotes a modified value of the material constant. In the present paper, the compressed notation from the IEEE standards for piezoceramic materials [24] has been used.

2.2. Linear field equations

The kinematic relations between the strain S and the displacements $u(x_1, x_3, t)$ and $w(x_1, x_3, t)$ in x_1 and x_3 directions, respectively, are given by

$$S_1 = u_{,1}, \quad S_3 = w_{,3} \quad \text{and} \quad S_5 = u_{,3} + w_{,1}. \tag{6}$$

Here the numbers (1,2,3) following the comma indicate differentiation with respect to (x_1, x_2, x_3), respectively (e.g. $u_{,3} = \partial u/\partial x_3$). The electric field E in terms of the electric potential $\varphi(x_1, x_3, t)$ is given by

$$E_1 = -\varphi_{,1} \quad \text{and} \quad E_3 = -\varphi_{,3}. \tag{7}$$

The field equations can be derived using Hamilton's principle [23], which for a piezoelectric continuum is

$$\delta \int_{t_0}^{t_1} L \, \mathrm{d}t + \int_{t_0}^{t_1} \delta W \, \mathrm{d}t = 0, \tag{8}$$

with the Lagrangian

$$L = \int_V (T - H) \, \mathrm{d}V, \tag{9}$$

where T denotes the kinetic energy density, H the electric enthalpy density, δW the virtual work and V the volume. However, the term H consists of purely mechanical, purely electrical and coupling terms but still it is termed as electric enthalpy density. The name electric enthalpy density was perhaps coined by Mason [25] and later it became standard in piezoceramic literature (e.g. IEEE standards [24]). In the conservative case, the electric enthalpy density H is defined through

$$T_p = \frac{\partial H}{\partial S_p} \quad \text{and} \quad D_i = -\frac{\partial H}{\partial E_i}. \tag{10}$$

Using Eqs. (1)–(5) and (10), the electric enthalpy density can be expressed as

$$\begin{aligned} H = {} & \tfrac{1}{2}\bar{c}_{11}S_1^2 + \tfrac{1}{2}\bar{c}_{33}S_3^2 + \tfrac{1}{2}c_{44}^E S_5^2 + \bar{c}_{13}S_1S_3 - \bar{e}_{31}S_1E_3 \\ & - \bar{e}_{33}S_3E_3 - e_{15}S_5E_1 - \tfrac{1}{2}\varepsilon_{11}^S E_1^2 - \tfrac{1}{2}\bar{\varepsilon}_{33}E_3^2. \end{aligned} \tag{11}$$

The kinetic energy is given by

$$\int_V T \, \mathrm{d}V = \tfrac{1}{2}\rho \int_V (\dot{u}^2 + \dot{w}^2) \, \mathrm{d}V, \tag{12}$$

where ρ is the density of the piezoceramic and a dot represents differentiation with respect to time t.

Energy terms are substituted in Hamilton's principle (8). Variation is performed with respect to δu, δw and $\delta\varphi$ and integration by parts is used. Collection of various terms in the integral signs

corresponding to the δu, δw and $\delta\varphi$ leads to the linear field equations

$$\rho\ddot{u} = \overline{c}_{11}u_{,11} + c_{44}^{E}u_{,33} + \left(\overline{c}_{13} + c_{44}^{E}\right)w_{,13} + (\overline{e}_{31} + e_{15})\varphi_{,13}, \tag{13}$$

$$\rho\ddot{w} = \overline{c}_{33}w_{,33} + c_{44}^{E}w_{,11} + \left(\overline{c}_{13} + c_{44}^{E}\right)u_{,13} + \overline{e}_{33}\varphi_{,33} + e_{15}\varphi_{,11}, \tag{14}$$

$$\varepsilon_{11}^{S}\varphi_{,11} + \overline{\varepsilon}_{33}\varphi_{,33} = (\overline{e}_{31} + e_{15})u_{,13} + e_{15}w_{,33} + \overline{e}_{33}w_{,33}, \tag{15}$$

with the corresponding boundary conditions (i.e. for clamped-free case $u = w = 0$ at $x_3 = -l/2$ and traction-free boundary conditions at all the free edges). The piezoceramic beam is used as an actuator and an external electric field is prescribed at the boundaries with electrodes (i.e. at $x_1 = -h/2, h/2$). It is appropriate here to assume that the electric potential in the piezoceramic vanishes at these boundaries [23]. Hence, electrodes are considered to be short-circuited in the present case (i.e. $\varphi = 0$ at $x_1 = -h/2, h/2$). For the un-electroded sides of the piezoceramic beam (i.e. at $x_3 = -l/2, l/2$), as the dielectric constant of the air is negligible in comparison to the dielectric constant of the piezoceramic material, the surface charge density is assumed to be zero [24]. In the case when piezoceramic is used as sensor, an open-circuit assumption is more appropriate for the electroded surfaces. For the field equations (13)–(15) with the given boundary conditions, no closed-form solution is known.

2.3. Rayleigh–Ritz method

Bhat [26] proposed the use of orthogonal polynomials in the Rayleigh–Ritz method to obtain the natural frequencies of rectangular plates with free edges. The first member of each set of polynomials is constructed to satisfy the appropriate equivalent beam boundary conditions. The higher orthogonal members of these polynomials are generated using the Gram–Schmidt process and automatically satisfy the geometric boundary conditions. It is observed that the higher members of the set do not satisfy the natural boundary conditions of the equivalent beam, thereby relaxing the over-restraint encountered in the use of true beam functions. Dickinson and Di Blasio [27] proposed even lower starting members as compared to those by Bhat. It is observed by Oosterhout et al. [28] that in the Rayleigh–Ritz method the orthogonalization of the polynomials by the Gram–Schmidt process results in a numerically stable process. It leads to high convergence rates and accurate solutions for the higher modes. In the present work, the above-mentioned method is extended for a piezoelectric continuum.

Assuming u, w and φ as

$$u(x_1, x_3, t) = U(x_1, x_3)\sin\omega t, \tag{16}$$

$$w(x_1, x_3, t) = W(x_1, x_3)\sin\omega t, \tag{17}$$

$$\varphi(x_1, x_3, t) = \Phi(x_1, x_3)\sin\omega t \tag{18}$$

and using Eqs. (6), (7) and (11), the maximum electric enthalpy can be expressed as

$$H_{\max} = \tfrac{1}{2}b\int_A \Big(\overline{c}_{11}U_{,1}^2 + \overline{c}_{33}W_{,3}^2 + c_{44}^{E}U_{,3}^2 + c_{44}^{E}W_{,1}^2 + 2\overline{c}_{13}U_{,1}W_{,3} + 2\overline{e}_{31}U_{,1}\Phi_{,3} + 2\overline{e}_{33}W_{,3}\Phi_{,3} + 2e_{15}U_{,3}\Phi_{,1} + 2e_{15}W_{,1}\Phi_{,1} + 2c_{44}^{E}U_{,3}W_{,1} - \varepsilon_{11}^{S}\Phi_{,1}^2 - \overline{\varepsilon}_{33}\Phi_{,3}^2\Big)\,\mathrm{d}A. \tag{19}$$

Here, ω is the circular frequency and A indicates the integration domain over the area $l \times h$ (i.e. from $-l/2$ to $l/2$ and $-h/2$ to $h/2$). Similarly, from Eq. (12), the maximum kinetic energy is

$$T_{\max} = \tfrac{1}{2}\rho b\omega^2 \int_A (U^2 + W^2)\,\mathrm{d}A. \tag{20}$$

For the free vibrations of the piezoceramic the displacement amplitudes U and W may be expressed as

$$U = \{G_1(x_1, x_3)\}^{\mathrm{T}}\{\mathrm{A}\}_{(i+1)(j+1)\times 1}, \quad W = \{G_2(x_1, x_3)\}^{\mathrm{T}}\{\mathrm{B}\}_{(m+1)(n+1)\times 1} \tag{21}$$

and the electric potential Φ may be expressed as

$$\Phi = \{G_3(x_1, x_3)\}^{\mathrm{T}}\{\mathrm{C}\}_{(r+1)(s+1)\times 1}, \tag{22}$$

where $\{\mathrm{A}\}, \{\mathrm{B}\}, \{\mathrm{C}\}$ are the unknown coefficient vectors and

$$\begin{aligned} \{G_1\}_{(i+1)(j+1)\times 1} &= (\{\beta\}\{\gamma\}^{\mathrm{T}})^S, \\ \{G_2\}_{(m+1)(n+1)\times 1} &= (\{\delta\}\{\zeta\}^{\mathrm{T}})^S, \\ \{G_3\}_{(r+1)(s+1)\times 1} &= (\{\theta\}\{\phi\}^{\mathrm{T}})^S \end{aligned} \tag{23}$$

with

$$\begin{aligned} \{\beta(x_1)\} &= [\beta_0, \beta_1, \ldots, \beta_i]^{\mathrm{T}}, \\ \{\gamma(x_3)\} &= [\gamma_0, \gamma_1, \ldots, \gamma_j]^{\mathrm{T}}, \\ \{\delta(x_1)\} &= [\delta_0, \delta_1, \ldots, \delta_m]^{\mathrm{T}}, \\ \{\zeta(x_3)\} &= [\zeta_0, \zeta_1, \ldots, \zeta_n]^{\mathrm{T}}, \\ \{\theta(x_1)\} &= [\theta_0, \theta_1, \ldots, \theta_r]^{\mathrm{T}}, \\ \{\phi(x_3)\} &= [\phi_0, \phi_1, \ldots, \phi_s]^{\mathrm{T}}. \end{aligned} \tag{24}$$

The $\beta_i(x_1)$, $\gamma_j(x_3)$, $\delta_m(x_1)$, $\zeta_n(x_3)$, $\theta_r(x_1)$ and $\phi_s(x_3)$ are appropriate polynomial functions $(i, j, m, n, r, s = 0, 1, 2, \ldots)$ satisfying the geometric boundary conditions. Starting functions for each of these terms, and the Gram–Schmidt process [26] to obtain the higher-order functions are given in Appendix A. The stacks operator $(.)^S$ maps an $(i+1)\times(j+1)$ matrix into an $(i+1)(j+1)\times 1$ column vector. The stack of the matrix is a column vector formed by stacking the columns of the matrix [29] .

Substituting the expression for U, W, Φ from Eqs. (21) and (22) in the maximum kinetic energy (20) and the maximum potential energy (19) (the resultant form is shown in Appendix B), and differentiating it with respect to the unknown coefficients $\{\mathrm{A}\}, \{\mathrm{B}\}, \{\mathrm{C}\}$ provide

$$\left\{\frac{\partial T_{\max}}{\partial \mathrm{coeff}}\right\} = \rho b\omega^2 \int_A \left(\begin{bmatrix} \{G_1\}\{G_1\}^{\mathrm{T}} & & \\ & \{G_2\}\{G_2\}^{\mathrm{T}} & \\ & & [\mathrm{zeros}] \end{bmatrix} \right) \mathrm{d}A \begin{Bmatrix} \mathrm{A} \\ \mathrm{B} \\ \mathrm{C} \end{Bmatrix} \tag{25}$$

and

$$\left\{\frac{\partial H_{\max}}{\partial \mathrm{coeff}}\right\} = b \int_A \left(\begin{bmatrix} [K_{\mathrm{mech}}] & [K_{\mathrm{piezo}}] \\ [K_{\mathrm{piezo}}]^{\mathrm{T}} & [K_{\mathrm{dielectric}}] \end{bmatrix} \right) \mathrm{d}A \begin{Bmatrix} \mathrm{A} \\ \mathrm{B} \\ \mathrm{C} \end{Bmatrix}. \tag{26}$$

Details of the matrices $[K_{\text{mech}}], [K_{\text{piezo}}]$ and $[K_{\text{dielectric}}]$ are given in Appendix C. In the resultant diagonal matrix obtained by differentiating the kinetic energy, the diagonal elements corresponding to the coefficients {C} are zero. Therefore, before solving the eigenvalue problem, it is reduced using the Guyan reduction. The reduced eigenvalue problem is obtained as

$$[[K] - \omega^2[M]] \begin{Bmatrix} \text{A} \\ \text{B} \end{Bmatrix} = 0, \tag{27}$$

where

$$[K] = b \int_A ([[K_{\text{mech}}] - [K_{\text{piezo}}][K_{\text{dielectric}}]^{-1}[K_{\text{piezo}}]^{\text{T}}])\, \text{d}A \tag{28}$$

and

$$[M] = \rho b \int_A \left(\begin{bmatrix} \{G_1\}\{G_1\}^{\text{T}} & \\ & \{G_2\}\{G_2\}^{\text{T}} \end{bmatrix} \right) \text{d}A. \tag{29}$$

After calculating the eigenvalues and eigenvectors from the reduced eigenvalue problem, coefficients {C} are calculated from

$$\{\text{C}\} = -[K_{\text{dielectric}}]^{-1}[K_{\text{piezo}}]^{\text{T}} \begin{Bmatrix} \text{A} \\ \text{B} \end{Bmatrix}. \tag{30}$$

2.4. Convergence study

To observe the convergence behavior, the same number of polynomials are taken for all the terms in both directions (i.e. $i = j = m = n = r = s$). For the calculation purpose, the material parameters for the piezoceramic PIC 255 supplied by the manufacturer and displayed in Table 2 are used. Table 1 displays the convergence behavior of the first four flexural natural frequencies N_k $(k = 1\text{–}4)$ of a cantilever piezoceramic beam of $18 \times 14 \times 8\,\text{mm}^3$ dimensions. It can be observed that the frequencies start to converge very rapidly and sufficient convergence is achieved by using eight polynomials in both directions. After this, the maximum change in the values of the

Table 1
Convergence study

No. of polynomials	N_1 (kHz)	N_2 (kHz)	N_3 (kHz)	N_4 (kHz)
3	9.735	39.042	94.755	121.506
4	9.601	37.417	85.595	114.110
5	9.600	37.278	79.020	111.469
6	9.599	37.253	78.560	107.996
7	9.598	37.250	78.450	107.831
8	9.597	37.248	78.440	107.705
9	9.596	37.247	78.437	107.696
10	9.595	37.246	78.435	107.693
11	9.595	37.245	78.434	107.692
12	9.595	37.245	78.433	107.692

frequencies is less than 0.02%. However, in the present paper ten polynomials are used, till complete convergence up to three significant digits after the decimal is achieved for the first natural frequency.

2.5. Mode shapes

The solution of the eigenvalue problem (27) provides the eigenvectors {A},{B}, which can be further used in Eq. (30) to obtain the coefficients {C}. Substituting these in Eqs. (21) and (22) provides the mode shape for the corresponding eigenvalue.

In Fig. 3, the first four flexural modes of the beam are displayed. In the Euler–Bernoulli beam theory, it is assumed that the straight lines normal to the mid-plane before deformation remain straight and normal to the mid-plane after deformation. However, in the Timoshenko beam theory the normality assumption of the Euler–Bernoulli beam theory is relaxed and the straight lines normal to the mid-plane before deformation are assumed to remain straight after deformation. It can be observed from Fig. 3 that both the normality and straightness assumptions are defied. Specially at higher modes, the bending of the lines is more pronounced (Fig. 3(d)). Hence, for very thick beams neither of the assumptions of these two theories hold at the higher modes.

Fig. 4 shows the distribution of the electric potential Φ along the thickness h and length l for the same modes. It can be observed from this figure that the distribution of the electric potential is

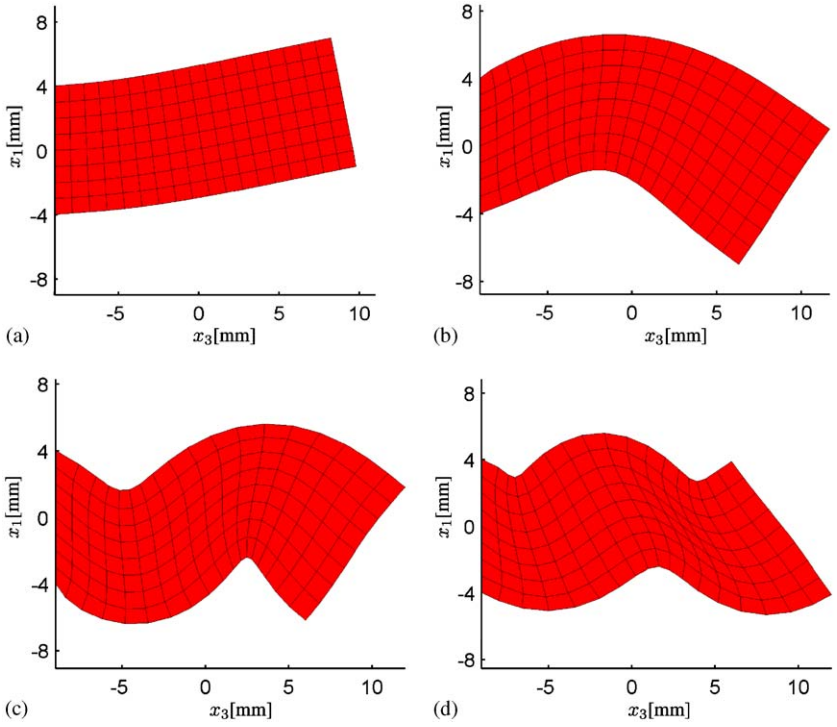

Fig. 3. Mode shapes for the $18 \times 14 \times 8\,\text{mm}^3$ test piece. (a) First flexural mode at 9.595 kHz; (b) second flexural mode at 37.246 kHz; (c) third flexural mode at 78.435 kHz; (d) fourth flexural mode at 107.693 kHz.

sinusoidal along the thickness direction for all the modes. To further understand the variation of the displacements U, W and the distribution of the electric potential Φ, two-dimensional plots for the first flexural mode are shown in Figs. 5 and 6. It can be seen from Fig. 5 that the electric potential Φ_k is sinusoidal along the thickness direction. The displacement W_k is linear and the displacement U_k has small variation (from 0.97 to 1.00) along the thickness. However, along the length direction, the variation of the U_k, W_k and the distribution of Φ_k are more involved (Fig. 6). The same is observed for the other higher modes. It can be noted that for the first mode electric potential diminishes rapidly along the length direction (Fig. 6(a)). Therefore, sinusoidal nature of

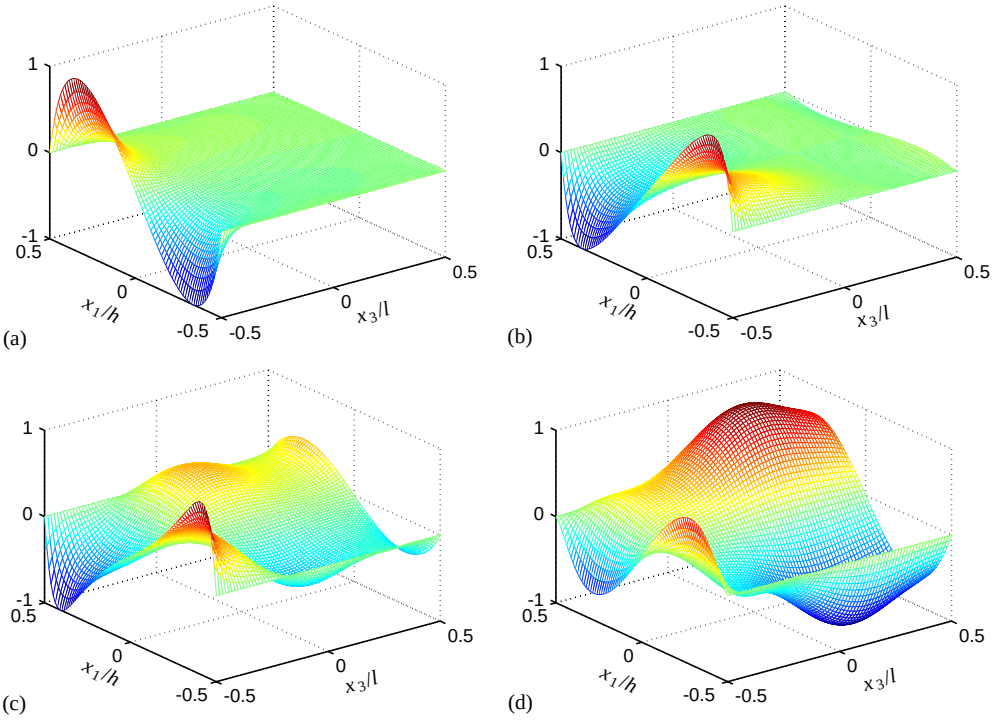

Fig. 4. Electric potential distribution for the $18 \times 14 \times 8\,\text{mm}^3$ test piece. (a) First flexural mode at 9.595 kHz; (b) second flexural mode at 37.246 kHz; (c) third flexural mode at 78.435 kHz; (d) fourth flexural mode at 107.693 kHz.

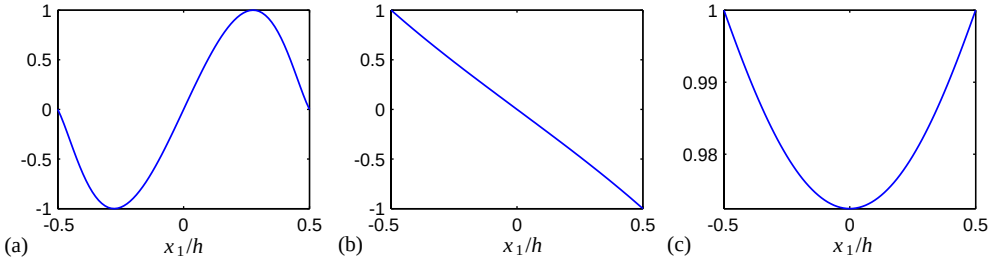

Fig. 5. Normalized variation along thickness: (a) Φ_k; (b) W_k; (c) U_k for first resonance, i.e. $k = 1$ ($x_3 = 0\,\text{mm}$).

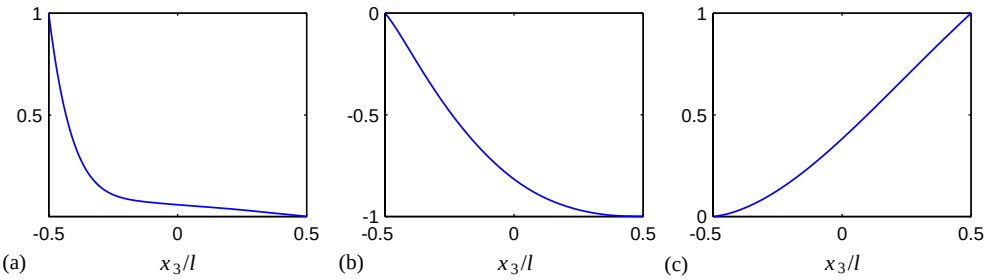

Fig. 6. Normalized variation along length: (a) Φ_k; (b) W_k; (c) U_k for first resonance, i.e. $k = 1$ ($x_1 = 2$ mm).

the electric potential along the thickness is not visible in Fig. 4(a) at the cross sections away from the fixed end. However, in a normalized plot, such as in Fig. 5(a), its sinusoidal nature can be easily verified for any cross section along the length of the beam.

For relatively thin beams, U_k may be assumed constant and W_k may be taken linear along the thickness, as assumed in the Timoshenko beam. Hence, the modified Timoshenko beam theory, which takes into account the sinusoidal distribution of the electric potential in the thickness direction and a more general distribution along the length direction, will be sufficient for the analysis of moderately thick beams. To model the vibration of the piezoelectric coupled structures excited using the d_{31} effect, Wang and Quek [30] and Liu et al. [31] used the same assumption to modify the Euler–Bernoulli beam theory and the Mindlin plate theory, respectively. A detailed analysis of nonlinear shear-induced flexural vibrations of piezoceramic beams using a modified Timoshenko beam theory and its comparison with the present work will be the subject of a future publication.

3. Nonlinear modeling

In order to model the nonlinear behavior observed in the experiments, the corresponding nonlinear constitutive relations are obtained in this section. Hamilton's principle together with the Ritz method are used to obtain a discretized equation of motion for a piezoceramic beam. The equation of motion is solved using perturbation analysis.

3.1. Nonlinear constitutive equations

In the experiments, when the piezoceramics are excited at one-third of the first resonance frequency, a superharmonic was observed at resonance frequency, revealing the presence of cubic nonlinearities. A similar experiment performed at one-half of the first resonance frequency showed the presence of quadratic nonlinearities of comparable order of magnitude. However, Parashar and von Wagner [6] and von Wagner [32] found that: based on experimental observations, if the quadratic nonlinearities are considered of the same order as that of the cubic, they do not appear in the first-order approximation of the perturbation solution. Hence, in the

present work, only the cubic nonlinearities are included in the model. The electric enthalpy term is extended to include fourth-order terms, such as

$$H = \tfrac{1}{2}\bar{c}_{11}S_1^2 + \tfrac{1}{2}\bar{c}_{33}S_3^2 + \tfrac{1}{2}c_{44}^E S_5^2 + \bar{c}_{13}S_1S_3 - \bar{e}_{31}S_1E_3 - \bar{e}_{33}S_3E_3 - e_{15}S_5E_1 - \tfrac{1}{2}\varepsilon_{11}^S E_1^2 - \tfrac{1}{2}\bar{\varepsilon}_{33}E_3^2 + \tfrac{1}{4}c_{44}^{(2)}S_5^4 - \tfrac{1}{3}e_{15}^{(1)}S_5^3E_1 - \tfrac{1}{2}e_{15}^{(2)}S_5^2E_1^2 - \tfrac{1}{3}e_{15}^{(3)}S_5E_1^3 - \tfrac{1}{4}\varepsilon_{11}^{(2)}E_1^4. \quad (31)$$

Here $c_{44}^{(2)}$ is the parameter of the cubic nondissipative elastic term, $e_{15}^{(1)}, e_{15}^{(2)}, e_{15}^{(3)}$ are the higher-order piezoelectric coupling parameters, and $\varepsilon_{11}^{(2)}$is the higher-order dielectric parameter. A comparable energy function is given by Maugin [33]. In addition to these conservative nonlinear terms, the constitutive relations are also extended by including dissipative linear [34] and nonlinear terms as

$$T_1 = \bar{c}_{11}S_1 + \bar{c}_{13}S_3 - \bar{e}_{31}E_3 + c_{11d}(\dot{S}_1) + c_{13d}(\dot{S}_3) - e_{31d}(\dot{E}_3), \quad (32)$$

$$T_3 = \bar{c}_{13}S_1 + \bar{c}_{33}S_3 - \bar{e}_{33}E_3 + c_{13d}(\dot{S}_1) + c_{33d}(\dot{S}_3) - e_{33d}(\dot{E}_3), \quad (33)$$

$$T_5 = c_{44}^E S_5 - e_{15}E_1 + c_{44d}(\dot{S}_5) - e_{15d}(\dot{E}_1) + c_{44}^{(2)}S_5^3 - e_{15}^{(1)}S_5^2E_1 - e_{15}^{(2)}S_5E_1^2 - \tfrac{1}{3}e_{15}^{(3)}E_1^3 + c_{44d}^{(2)}(\dot{S}_5^3) - e_{15d}^{(1)}(\dot{S_5^2E_1}) - e_{15d}^{(2)}(\dot{S_5E_1^2}) - \tfrac{1}{3}e_{15d}^{(3)}(\dot{E}_1^3), \quad (34)$$

$$D_1 = \varepsilon_{11}^S E_1 + e_{15}S_5 + \varepsilon_{11d}(\dot{E}_1) + e_{15d}(\dot{S}_5) + \tfrac{1}{3}e_{15}^{(1)}S_5^3 + e_{15}^{(2)}S_5^2E_1 + e_{15}^{(3)}S_5E_1^2 + \varepsilon_{11}^{(2)}E_1^3 + \tfrac{1}{3}e_{15d}^{(1)}(\dot{S}_5^3) + e_{15d}^{(2)}(\dot{S_5^2E_1}) + e_{15d}^{(3)}(\dot{S_5E_1^2}) + \varepsilon_{11d}^{(2)}(\dot{E}_1^3), \quad (35)$$

$$D_3 = \bar{\varepsilon}_{33}E_3 + \bar{e}_{31}S_1 + \bar{e}_{33}S_3 + \varepsilon_{33d}(\dot{E}_3) + e_{31d}(\dot{S}_1) + e_{33d}(\dot{S}_3), \quad (36)$$

where c_{11d}, c_{13d}, c_{33d}, c_{44d}, e_{31d}, e_{33d}, e_{15d}, ε_{11d}, ε_{33d} are linear dissipative parameters, $c_{44d}^{(2)}$ is the parameter of the cubic dissipative mechanical term, $\varepsilon_{11d}^{(2)}$ is the corresponding dielectric parameter, and $e_{15d}^{(1)}, e_{15d}^{(2)}, e_{15d}^{(3)}$ are the higher-order parameters for the dissipative piezoelectric coupling.

Based on the observations [9] of free piezoceramic vibrations using the d_{15} effect, here only the constitutive relations for the T_5 and D_1 are extended to include the cubic-order terms. It was observed that the main nonlinearities stem from these two constitutive relations only. Even though all other constitutive relations can be similarly extended, it is not possible to determine all the individual parameters uniquely in the present analysis.

3.2. Nonlinear equation of motion

The nonlinear electric enthalpy density from Eq. (31), the kinetic energy from Eq. (12), together with the δW term obtained from the constitutive relations (32)–(36) are used in Hamilton's principle (8), to obtain the nonlinear equation of motion.

As described in Section 2.3, using the Rayleigh–Ritz method, the circular eigenfrequencies ω_k $(k = 1, 2, 3, \ldots)$ and the corresponding eigenfunctions (U_k, W_k, Φ_k) can be obtained. Using

these eigenfunctions, approximate solutions are represented by

$$u(x_1, x_3, t) = \sum_k U_k(x_1, x_3) p_k(t), \tag{37}$$

$$w(x_1, x_3, t) = \sum_k W_k(x_1, x_3) p_k(t), \tag{38}$$

$$\varphi(x_1, x_3, t) = \sum_k \Phi_k(x_1, x_3) p_k(t) + \frac{U_0}{h} x_1 \cos \Omega t. \tag{39}$$

Here U_0 is the excitation voltage amplitude and Ω is the circular excitation frequency. The Ritz method with only one eigenfunction, namely the eigenfunction close to the excitation frequency, is used for the discretization by von Wagner and Hagedorn [35] in a piezo-beam system. For comparison, the calculations with up to four shape functions were performed considering full nonlinear coupling. The results showed good agreement, with the eigenfunctions of the linearized problem used as shape functions. Keeping this in mind, the following simplified solutions are used in Ritz method for the discretization:

$$u(x_1, x_3, t) = U_k(x_1, x_3) p_k(t), \tag{40}$$

$$w(x_1, x_3, t) = W_k(x_1, x_3) p_k(t), \tag{41}$$

$$\varphi(x_1, x_3, t) = \Phi_k(x_1, x_3) p_k(t) + \frac{U_0}{h} x_1 \cos \Omega t \tag{42}$$

for the system excited close to the kth resonance frequency.

Introducing Eqs. (40)–(42) in Hamilton's principle leads to the discretized nonlinear equation of motion for the piezoceramic beam as

$$\begin{aligned} &m_k \ddot{p_k} + d_k \dot{p_k} + c_k^{(1)} p_k + c_k^{(2)} p_k^3 + c_{kd}^{(2)} p_k^2 \dot{p_k} \\ &\quad = f_k^{(1)} \cos \Omega t - f_{kd}^{(1)} \Omega \sin \Omega t + f_k^{(2)} \cos \Omega t p_k^2 + 2 f_{kd}^{(2)} \cos \Omega t p_k \dot{p_k} \\ &\qquad - f_{kd}^{(2)} \Omega \sin \Omega t p_k^2 + f_k^{(3)} \cos^2 \Omega t p_k + f_{kd}^{(3)} \cos^2 \Omega t \dot{p_k} - 2 f_{kd}^{(3)} \Omega \cos \Omega t \sin \Omega t p_k \\ &\qquad + f_k^{(4)} \cos^3 \Omega t - 3 f_{kd}^{(4)} \Omega \cos^2 \Omega t \sin \Omega t \end{aligned} \tag{43}$$

with

$$m_k = \rho \int_A \left(U_k^2 + W_k^2\right) \mathrm{d}A,$$

$$\begin{aligned} d_k = \int_A \Big(& c_{11d} U_{k,1}^2 + c_{33d} W_{k,3}^2 + 2 c_{13d} U_{k,1} W_{k,3} + 2 e_{31d} U_{k,1} \Phi_{k,3} + 2 e_{33d} W_{k,3} \Phi_{k,3} - \varepsilon_{33d} \Phi_{k,3}^2 \\ & + c_{44d} (U_{k,3} + W_{k,1})^2 + 2 e_{15d} (U_{k,3} + W_{k,1}) \Phi_{k,1} - \varepsilon_{11d} \Phi_{k,1}^2 \Big) \mathrm{d}A, \end{aligned}$$

$$\begin{aligned} c_k^{(1)} = \int_A \Big(& \overline{c}_{11} U_{k,1}^2 + \overline{c}_{33} W_{k,3}^2 + 2 \overline{c}_{13} U_{k,1} W_{k,3} + 2 \overline{e}_{31} U_{k,1} \Phi_{k,3} + 2 \overline{e}_{33} W_{k,3} \Phi_{k,3} - \overline{\varepsilon}_{33} \Phi_{k,3}^2 \\ & + c_{44}^E (U_{k,3} + W_{k,1})^2 + 2 e_{15} (U_{k,3} + W_{k,1}) \Phi_{k,1} - \varepsilon_{11}^S \Phi_{k,1}^2 \Big) \mathrm{d}A, \end{aligned}$$

$$
\begin{aligned}
c_k^{(2)} &= \int_A \Big(c_{44}^{(2)}(U_{k,3}+W_{k,1})^4 + \tfrac{4}{3}e_{15}^{(1)}(U_{k,3}+W_{k,1})^3\Phi_{k,1} \\
&\quad -2e_{15}^{(2)}(U_{k,3}+W_{k,1})^2\Phi_{k,1}^2 + \tfrac{4}{3}e_{15}^{(3)}(U_{k,3}+W_{k,1})\Phi_{k,1}^3 - \varepsilon_{11}^{(2)}\Phi_{k,1}^4 \Big)\,\mathrm{d}A, \\
c_{kd}^{(2)} &= \int_A \Big(3c_{44d}^{(2)}(U_{k,3}+W_{k,1})^4 + 4e_{15d}^{(1)}(U_{k,3}+W_{k,1})^3\Phi_{k,1} \\
&\quad -6e_{15d}^{(2)}(U_{k,3}+W_{k,1})^2\Phi_{k,1}^2 + 4e_{15d}^{(3)}(U_{k,3}+W_{k,1})\Phi_{k,1}^3 - 3\varepsilon_{11d}^{(2)}\Phi_{k,1}^4 \Big)\,\mathrm{d}A, \\
f_k^{(1)} &= \frac{U_0}{h}\int_A \big(-e_{15}(U_{k,3}+W_{k,1}) + \varepsilon_{11}^S\Phi_{k,1}\big)\,\mathrm{d}A, \\
f_{kd}^{(1)} &= \frac{U_0}{h}\int_A (-e_{15d}(U_{k,3}+W_{k,1}) + \varepsilon_{11d}\Phi_{k,1})\,\mathrm{d}A, \\
f_k^{(2)} &= \frac{U_0}{h}\int_A \Big(-e_{15}^{(1)}(U_{k,3}+W_{k,1})^3 + 3e_{15}^{(2)}(U_{k,3}+W_{k,1})^2\Phi_{k,1} \\
&\quad -3e_{15}^{(3)}(U_{k,3}+W_{k,1})\Phi_{k,1}^2 + 3\varepsilon_{11}^{(2)}\Phi_{k,1}^3 \Big)\,\mathrm{d}A, \\
f_{kd}^{(2)} &= \frac{U_0}{h}\int_A \Big(-e_{15d}^{(1)}(U_{k,3}+W_{k,1})^3 + 3e_{15d}^{(2)}(U_{k,3}+W_{k,1})^2\Phi_{k,1} \\
&\quad -3e_{15d}^{(3)}(U_{k,3}+W_{k,1})\Phi_{k,1}^2 + 3\varepsilon_{11d}^{(2)}\Phi_{k,1}^3 \Big)\,\mathrm{d}A, \\
f_k^{(3)} &= \frac{U_0^2}{h^2}\int_A \Big(e_{15}^{(2)}(U_{k,3}+W_{k,1})^2 - 2e_{15}^{(3)}(U_{k,3}+W_{k,1})\Phi_{k,1} + 3\varepsilon_{11}^{(2)}\Phi_{k,1}^2 \Big)\,\mathrm{d}A, \\
f_{kd}^{(3)} &= \frac{U_0^2}{h^2}\int_A \Big(e_{15d}^{(2)}(U_{k,3}+W_{k,1})^2 - 2e_{15d}^{(3)}(U_{k,3}+W_{k,1})\Phi_{k,1} + 3\varepsilon_{11d}^{(2)}\Phi_{k,1}^2 \Big)\,\mathrm{d}A, \\
f_k^{(4)} &= \frac{U_0^3}{h^3}\int_A \Big(-\tfrac{1}{3}e_{15}^{(3)}(U_{k,3}+W_{k,1}) + \varepsilon_{11}^{(2)}\Phi_{k,1} \Big)\,\mathrm{d}A, \\
f_{kd}^{(4)} &= \frac{U_0^3}{h^3}\int_A \Big(-\tfrac{1}{3}e_{15d}^{(3)}(U_{k,3}+W_{k,1}) + \varepsilon_{11d}^{(2)}\Phi_{k,1} \Big)\,\mathrm{d}A.
\end{aligned}
\tag{44}
$$

3.3. Solution by perturbation analysis

An approximate solution of the nonlinear equation of motion (43) is obtained using perturbation analysis. For the perturbation analysis, we define a nondimensional time

$$\tau = \omega_0 t \quad \text{with } \omega_0 = \sqrt{c_k^{(1)}/m_k}, \tag{45}$$

as well as the frequency ratio

$$\eta = \frac{\Omega}{\omega_0}. \tag{46}$$

Using Eqs. (45) and (46), the equation of motion (43) can be expressed as

$$\begin{aligned} &p'' + \varepsilon\kappa p' + p + \varepsilon\alpha_1 p^3 + \varepsilon\alpha_{1d} p^2 p' \\ &\quad = \varepsilon q(h_1 \cos\eta\tau + h_2 \sin\eta\tau) + \varepsilon q_d \eta(-h_2 \cos\eta\tau + h_1 \sin\eta\tau) + \varepsilon\alpha_2 p^2 (h_1 \cos\eta\tau + h_2 \sin\eta\tau) \\ &\qquad + 2\varepsilon\alpha_{2d} p p' (h_1 \cos\eta\tau + h_2 \sin\eta\tau) - \varepsilon\alpha_{2d} p^2 \eta(-h_2 \cos\eta\tau + h_1 \sin\eta\tau) \\ &\qquad + \varepsilon^2\alpha_3 p (h_1 \cos\eta\tau + h_2 \sin\eta\tau)^2 + \varepsilon^2\alpha_{3d} p' (h_1 \cos\eta\tau + h_2 \sin\eta\tau)^2 \\ &\qquad - 2\varepsilon^2\alpha_{3d} p \eta(h_1 \cos\eta\tau + h_2 \sin\eta\tau)(-h_2 \cos\eta\tau + h_1 \sin\eta\tau) + \varepsilon^3\alpha_4 (h_1 \cos\eta\tau + h_2 \sin\eta\tau)^3 \\ &\qquad - 3\varepsilon^3\alpha_{4d} \eta(h_1 \cos\eta\tau + h_2 \sin\eta\tau)^2(-h_2 \cos\eta\tau + h_1 \sin\eta\tau) \end{aligned} \tag{47}$$

with

$$()' = \frac{\mathrm{d}}{\mathrm{d}\tau}, \quad \kappa = \frac{d_k}{\varepsilon m_k \omega_0}, \quad q = \frac{f_k^{(1)}}{\varepsilon m_k \omega_0^2}, \quad q_d = \frac{-f_{kd}^{(1)}}{\varepsilon m_k \omega_0},$$

$$\alpha_1 = \frac{c_k^{(2)}}{\varepsilon m_k \omega_0^2}, \quad \alpha_{1d} = \frac{c_{kd}^{(2)}}{\varepsilon m_k \omega_0},$$

$$\alpha_2 = \frac{f_k^{(2)}}{\varepsilon m_k \omega_0^2}, \quad \alpha_{2d} = \frac{f_{kd}^{(2)}}{\varepsilon m_k \omega_0}, \quad \alpha_3 = \frac{f_k^{(3)}}{\varepsilon^2 m_k \omega_0^2}, \quad \alpha_{3d} = \frac{f_{kd}^{(3)}}{\varepsilon^2 m_k \omega_0},$$

$$\alpha_4 = \frac{f_k^{(4)}}{\varepsilon^3 m_k \omega_0^2}, \quad \alpha_{4d} = \frac{f_{kd}^{(4)}}{\varepsilon^3 m_k \omega_0}.$$

Here the coefficients h_1 and h_2 are introduced to allow for a phase shift between the excitation and the response of the system. The parameter ε can be chosen arbitrarily, but has to be small. Now, the Lindstedt–Poincaré method is used with

$$p = p_0 + \varepsilon p_1 + \cdots, \quad \eta = 1 + \varepsilon\eta_1 + \cdots . \tag{48}$$

Introducing Eq. (48) into Eq. (47) for the zeroth order results in

$$p_0'' + \eta^2 p_0 = 0, \tag{49}$$

and for the first order in

$$\begin{aligned} p_1'' + \eta^2 p_1 = &- \kappa p_0' + 2\eta_1 p_0 - \alpha_1 p_0^3 - \alpha_{1d} p_0^2 p_0' \\ &+ q(h_1 \cos\eta\tau + h_2 \sin\eta\tau) + q_d \eta(-h_2 \cos\eta\tau + h_1 \sin\eta\tau) \\ &+ \alpha_2 p_0^2 (h_1 \cos\eta\tau + h_2 \sin\eta\tau) + 2\alpha_{2d} p_0 p_0' (h_1 \cos\eta\tau + h_2 \sin\eta\tau) \\ &- \alpha_{2d} p_0^2 \eta(-h_2 \cos\eta\tau + h_1 \sin\eta\tau). \end{aligned} \tag{50}$$

The solution of Eq. (49) is given by

$$p_0 = P \cos\eta\tau \tag{51}$$

with unknown amplitude P. Using Eq. (51) in Eq. (50), the condition of vanishing secular terms leads to

$$2\eta_1 P - \tfrac{3}{4}\alpha_1 P^3 + (q + \tfrac{3}{4}\alpha_2 P^2)h_1 + (-q_d + \tfrac{1}{4}\alpha_{2d} P^2)\eta h_2 = 0, \tag{52}$$

$$\kappa\eta P + \tfrac{1}{4}\alpha_{1d}\eta P^3 + (q_d - \tfrac{3}{4}\alpha_{2d} P^2)\eta h_1 + (q + \tfrac{1}{4}\alpha_2 P^2)h_2 = 0. \tag{53}$$

These two algebraic equations, along with the condition $h_1^2 + h_2^2 = 1$, yield a polynomial equation of fifth order in terms of P^2

$$a_5 P^{10} + a_4 P^8 + a_3 P^6 + a_2 P^4 + a_1 P^2 + a_0 = 0, \tag{54}$$

which can be solved using MATLAB®. The roots of this polynomial provide values of the amplitude.

3.4. Calculation of the electric current

To get further information about the behavior of the piezoceramic, the electric current in the piezoceramic is measured with the help of a resistance in series. In the model, the electric current at one electrode is given by

$$I(t) = \frac{\mathrm{d}Q}{\mathrm{d}t} = -\frac{\mathrm{d}}{\mathrm{d}t}\int_F D_1 \,\mathrm{d}F, \tag{55}$$

where F is the area of an electrode. Using the constitutive equation (35), the amplitude of the electric current can be calculated if the displacement response including the amplitude and the phase shift are known. This is done symbolically using the MATLAB® 6.5 Symbolic toolbox.

4. Experimental setup

The experiments are carried out using cantilever piezoceramic beams of length $l = 18$ mm, width $b = 14$ mm and of two different thicknesses: $h = 8$, 3 mm. The piezoceramic beams are excited close to the first flexural resonance, by a computer-controlled gain-phase analyzer (Hewlett-Packard HP 4194A). The gain-phase analyzer applies a frequency sweep and simultaneously records the gain. The excitation signals from the gain-phase analyzer are amplified by the power amplifier (Brüel and Kjaer 2713), before being fed to the piezoceramic. A digital oscilloscope (Yokogawa DL708E) is used to monitor the excitation voltage amplitude and responses. The vibrations of the piezoceramic are measured with the help of a laser vibrometer (Polytec). The laser vibrometer has two units (viz. optic unit and electronic unit). The optic unit (OFV508) supplies the laser signals, and simultaneously senses the reflected signal. The reflected signals are then processed by the electronic unit (OFV2802), and fed to the test channel of the gain phase analyzer. The output of the power amplifier is also fed to the reference channel of the gain-phase analyzer to measure the gain.

In order to measure the current flowing through the piezoceramic at different excitation frequencies, the standard method described in Ikeda [34] (constant voltage method) is used. A low-value resistance (shunt of $r = 0.5\,\Omega$) is placed in series with the piezoceramic. The laser vibrometer circuit is then disconnected, and the voltage signals from the shunt are fed to the test

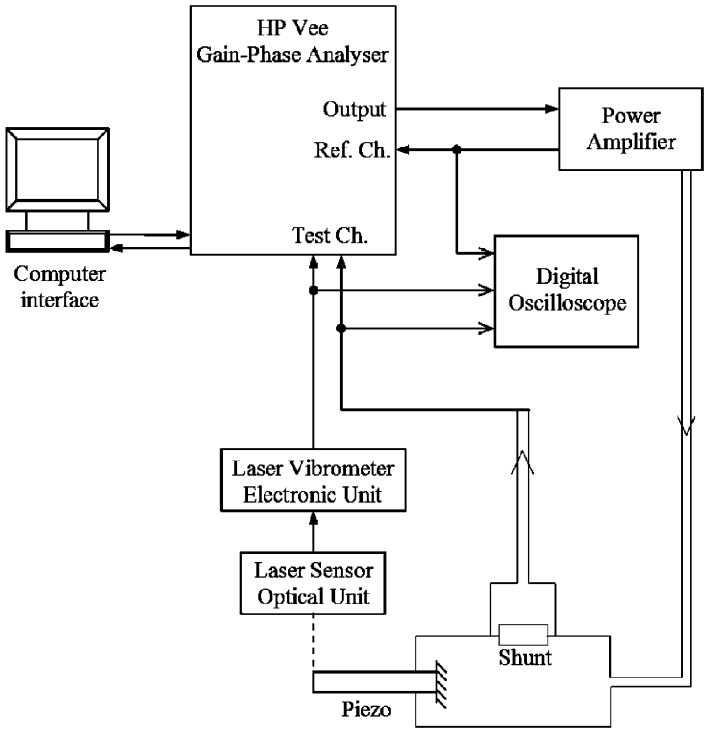

Fig. 7. Experimental setup.

channel of the gain-phase analyzer. The voltage at this shunt is very small compared to the excitation voltage and does not influence the applied voltage. Several shunts with different resistance values were also used and no significant influence on the current measurement was observed. All the shunts used were having resistance values several orders smaller than the impedance of the piezoceramic at resonance frequency as recommended in Ikeda [34] (i.e. $|Z|/r \geqslant 100$). The experimental setup for the same is shown in Fig. 7.

5. Parameter identification and experimental verification

In the present work, piezoceramic cantilever beams of the material PIC 255 supplied by PI Ceramic, Lederhose, Germany are used. The linear and nonlinear parameters are obtained for the piezoceramics by fitting the experimental and model results. The *fminsearch* command of MATLAB® 6.5 (based on Nelder–Mead simplex search method) is used to find here the optimized values of various parameters.

5.1. Linear parameters

In the first step, the linear parameters are identified by fitting the normalized displacement amplitude curve and the normalized current amplitude curve for the approximate linear behavior

at $U_0 = 2\,\mathrm{V}$. The linear identified parameters along with the approximate parameters supplied by the manufacturer are shown in Table 2. All the identified parameters are close to the manufacturer-supplied values, except for the parameter ε_{11}^S, which has around 50% variation. A small variation of 10% can also be observed between some of the identified parameters for $h = 8\,\mathrm{mm}$ and $h = 3\,\mathrm{mm}$. According to the manufacturer, the samples with different thicknesses may have been produced from different charges of raw material, which could explain for this variation.

It can be observed from the expression of the linear damping d_k in Eq. (44) that it is linearly dependent on nine material parameters. Therefore, various combinations of these parameters are possible to obtain the same results. To demonstrate this, for the piezoceramics with $h = 8\,\mathrm{mm}$, the dissipative mechanical and dielectric parameters are optimized, and dissipative piezoelectric coupling terms are assumed as zero. The resulting parameters are given in Table 3. Fig. 8 shows the theoretical and experimental normalized displacement responses $u(h/2, l/2)/U_0$, at 2 V excitation voltage and at the first resonance. Fig. 9 shows the normalized current responses for the same. It can be observed from these two figures that, with the identified linear parameters, the theoretical response is in good agreement with the experimental results. At low voltage excitation the current measured in the piezoceramic is of very small magnitude. Hence, for the normalized current response some noise is observed in the measured data due to the instrument noise. However, the theoretical response matches fairly well with measured data along the whole frequency range. At higher voltage excitation the current measured in the piezoceramic is of relatively large magnitude than that of instrument noise. Hence, the noise disappears.

Table 2
Linear material parameters

	Manufacturer's values	$18 \times 14 \times 8\,\mathrm{mm}^3$	$18 \times 14 \times 3\,\mathrm{mm}^3$
ρ (kg/m^3)	7800	7800	7800
c_{11}^E (N/m^2)	1.108×10^{11}	1.084×10^{11}	1.092×10^{11}
c_{12}^E (N/m^2)	6.326×10^{10}	6.326×10^{10}	6.326×10^{10}
c_{13}^E (N/m^2)	6.896×10^{10}	7.162×10^{10}	6.980×10^{10}
c_{33}^E (N/m^2)	1.108×10^{11}	1.084×10^{11}	1.092×10^{11}
c_{44}^E (N/m^2)	1.909×10^{10}	1.909×10^{10}	1.909×10^{10}
e_{31} (N/mV)	−5.6	−5.6	−5.6
e_{33} (N/mV)	12.8	12.8	12.8
e_{15} (N/mV)	10.3	9.8	8.02
$\varepsilon_{33}^S/\varepsilon_0$	1161	1161	1161
$\varepsilon_{11}^S/\varepsilon_0$	1023	1582	1653

Table 3
Linear damping parameters, $h = 8\,\mathrm{mm}$

c_{11d} (N s/m^2)	c_{13d} (N s/m^2)	c_{33d} (N s/m^2)	c_{44d} (N s/m^2)	ε_{33d} (N s/V^2)	ε_{11d} (N s/V^2)
6000	−9000	290	5800	-1.0×10^{-14}	-1.0×10^{-14}

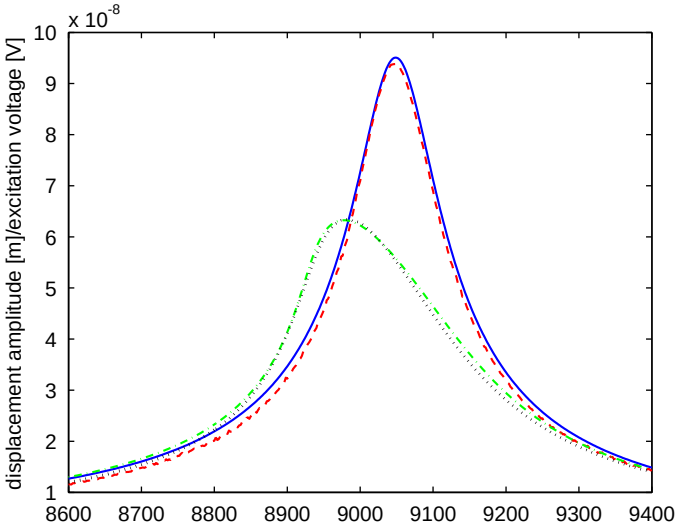

Fig. 8. Normalized displacement response for the beam with $h = 8$ mm at various excitation voltages (electric field strengths): — theory 2 V (0.25 V/mm); – – – experiment 2 V (0.25 V/mm); – · – · – theory 25 V (3.125 V/mm); · · · · · experiment 25 V (3.125 V/mm).

For the piezoceramic with $h = 3$ mm, the dissipative dielectric parameters are assumed as zero and the elastic and piezoelectric dissipative parameters are optimized. Table 4 displays the identified parameters. From Fig. 10 for the normalized displacement response and Fig. 11 for the normalized current response, it is evident that identified parameters can simulate the experimental results at low voltage values.

5.2. Nonlinear parameters

To identify the nonlinear parameters, experimental results at 25 V are compared with the model. The term $c_k^{(2)}$ in the nonlinear equation of motion can give rise to the observed softening nonlinear behavior in the experiments. It was shown in Ref. [36] that the term with combined parametric excitation and nonlinearity $f_k^{(2)}$ can produce the decrease of the normalized amplitude. Both the terms are rewritten here as

$$c_k^{(2)} = \int_A \Big(c_{44}^{(2)}(U_{k,3} + W_{k,1})^4 + \tfrac{4}{3} e_{15}^{(1)}(U_{k,3} + W_{k,1})^3 \Phi_{k,1} - 2e_{15}^{(2)}(U_{k,3} + W_{k,1})^2 \Phi_{k,1}^2 + \tfrac{4}{3} e_{15}^{(3)}(U_{k,3} + W_{k,1}) \Phi_{k,1}^3 - \varepsilon_{11}^{(2)} \Phi_{k,1}^4 \Big) \, \mathrm{d}A,$$

$$f_k^{(2)} = \frac{U_0}{h} \int_A \Big(-e_{15}^{(1)}(U_{k,3} + W_{k,1})^3 + 3e_{15}^{(2)}(U_{k,3} + W_{k,1})^2 \Phi_{k,1} - 3e_{15}^{(3)}(U_{k,3} + W_{k,1}) \Phi_{k,1}^2 + 3\varepsilon_{11}^{(2)} \Phi_{k,1}^3 \Big) \, \mathrm{d}A.$$

It can be seen from these expressions that $f_k^{(2)}$ is linearly dependent on the four higher-order cubic parameters, which also appear in the expression of $c_k^{(2)}$. The term $c_k^{(2)}$ additionally depends on the

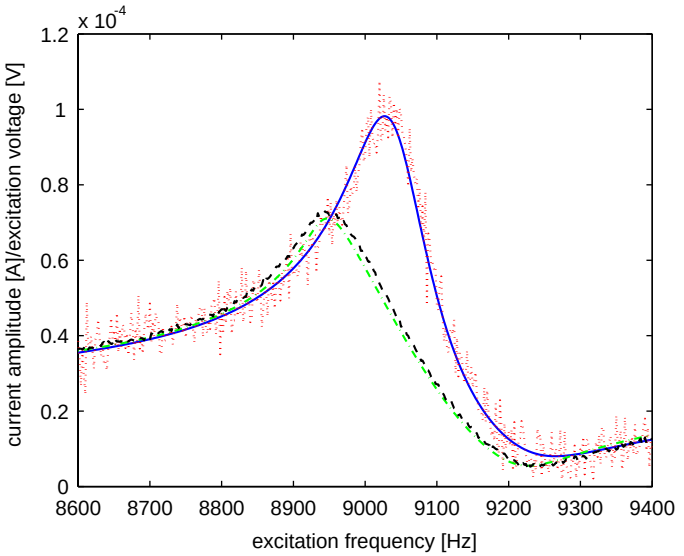

Fig. 9. Normalized current response for the beam with $h = 8$ mm at various excitation voltages (electric field strengths): — theory 2 V (0.25 V/mm); · · · · · experiment 2 V (0.25 V/mm); – · – · – theory 25 V (3.125 V/mm); – – – experiment 25 V (3.125 V/mm).

Table 4
Linear damping parameters, $h = 3$ mm

c_{11d} (N s/m^2)	c_{13d} (N s/m^2)	c_{33d} (N s/m^2)	c_{44d} (N s/m^2)	e_{31d} (N s/mV)	e_{33d} (N s/mV)
6000	−9000	290	5800	-8.8×10^{-4}	-1.0×10^{-4}

higher-order elastic parameter $c_{44}^{(2)}$. Clearly, it is not possible to determine all the five cubic parameters uniquely. Similarly, the terms $c_{kd}^{(2)}$ and $f_{kd}^{(2)}$ responsible for nonlinear damping are linearly dependent on five higher-order dissipative parameters.

It is shown by Parashar et al. [9] that, choosing only one parameter each from the dissipative and conservative higher-order terms, it is possible to simulate the experimental results. However, choosing only the piezoelectric coupling parameter will not be thermodynamically consistent [6,32]. It is observed by von Wagner and Hagedorn [35] for the piezo-beam systems that there is nonlinear elastic behavior in those piezoceramics. Keeping this in mind, for the piezoceramic with $h = 8$ mm, conservative nonlinear parameters $c_{44}^{(2)}$, $\varepsilon_{11}^{(2)}$ and dissipative nonlinear parameters $c_{44d}^{(2)}$, $\varepsilon_{11d}^{(2)}$ are optimized. For the piezoceramic with $h = 3$ mm, a different set consisting the conservative nonlinear parameters $c_{44}^{(2)}, e_{15}^{(1)}$ and dissipative nonlinear parameters $c_{44d}^{(2)}, e_{15d}^{(1)}$ is taken. The optimized parameters are shown in Tables 5 and 6. Using identified linear and nonlinear parameters, the results of the theoretical model are compared with the experimental results at 25 V. Figs. 8 and 9 for $h = 8$ mm, and Figs. 10 and 11 for $h = 3$ mm show a good agreement between the experiments and theoretical model.

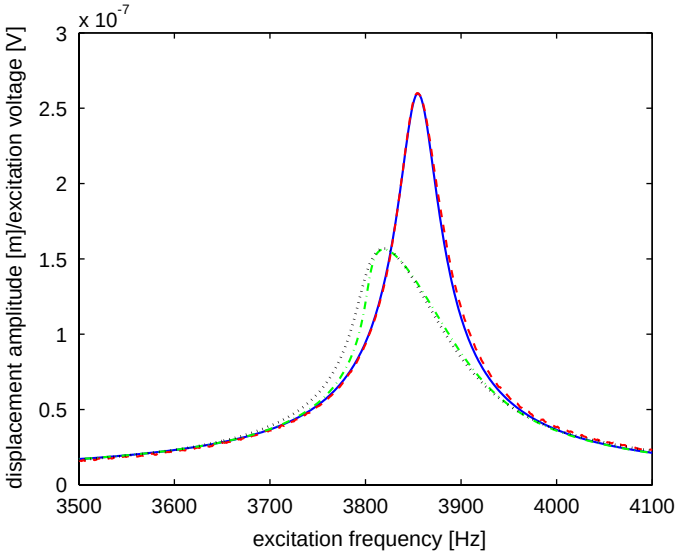

Fig. 10. Normalized displacement response for the beam with $h = 3$ mm at various excitation voltages (electric field strengths): — theory 2 V (0.666 V/mm); – – – experiment 2 V (0.666 V/mm); – · – · – theory 25 V (8.333 V/mm); · · · · · experiment 25 V (8.333 V/mm).

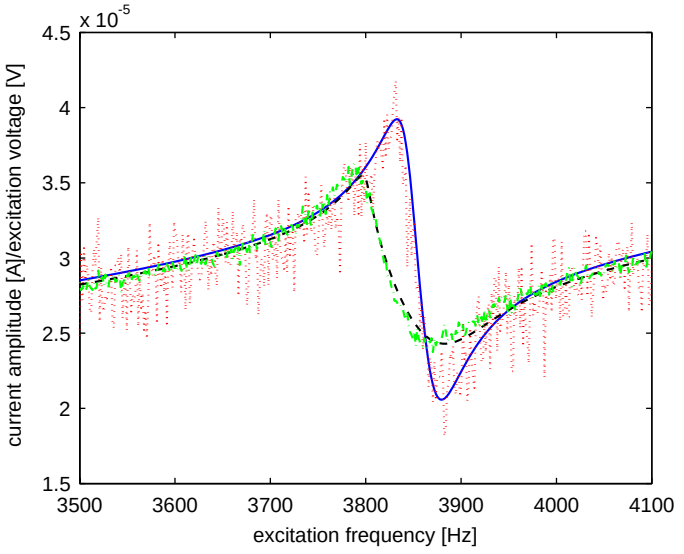

Fig. 11. Normalized current response for the beam with $h = 3$ mm at various excitation voltages (electric field strengths): — theory 5 V (1.666 V/mm); · · · · · experiment 5 V (1.666 V/mm); – – – theory 25 V (8.333 V/mm); – · – · – experiment 25 V (8.333 V/mm).

It is worth mentioning here that the Eq. (54) given in Section 3.3 and used for computing displacement amplitude will have five real solutions in general. For the parameters used in the present case, there will only be three real solutions. The intermediate solution from these three

Table 5
Nonlinear material parameters, $h = 8\,\text{mm}$

$c_{44}^{(2)}$ (N/m^2)	$c_{44d}^{(2)}$ (N s/m^2)	$\varepsilon_{11}^{(2)}$ (N/V^2)	$\varepsilon_{11d}^{(2)}$ (N s/V^2)
-5.8×10^{18}	4.4×10^{13}	-5.0×10^{-19}	-1.1×10^{-24}

Table 6
Nonlinear material parameters, $h = 3\,\text{mm}$

$c_{44}^{(2)}$ (N/m^2)	$c_{44d}^{(2)}$ (N s/m^2)	$e_{15}^{(1)}$ (N/mV)	$e_{15d}^{(1)}$ (N s/mV)
-1.6×10^{20}	2.3×10^{15}	-1.5×10^{10}	7.5×10^{2}

solutions is known to be unstable and cannot be observed in the experiments [37]. The remaining two solutions provide the sweep-up and sweep-down amplitudes. However, in the present case, due to the high damping of the piezoceramic material PIC 255 the jump phenomenon is not visible as observed in the case of PIC 181 material [6–8] and both the solutions coincide.

6. Summary and conclusions

Typical nonlinear effects were observed in the experiments conducted with piezoceramic cantilever beams subjected to weak electric fields. These nonlinear effects indicate a softening behavior, and the reduction of normalized amplitudes with increase in the excitation voltage.

To model such a nonlinear behavior, first a reduced set of linear constitutive relations is used. Eigenvalues and eigenfunctions of the beam were determined using the Rayleigh–Ritz method. The methodology proposed by Bhat [26], to use the characteristic orthogonal polynomials in the Rayleigh–Ritz method, was here extended to a piezoelectric continuum. A convergence study was carried out to observe the convergence behavior of the used polynomials. The mode shapes for the first four flexural eigenfrequencies were plotted. It was observed that for the present case the assumptions of neither the Euler–Bernoulli beam theory nor the Timoshenko beam theory hold at higher modes. The electric potential distribution at first four flexural modes was also studied. A sinusoidal distribution of the electric potential along the thickness and more general distribution along the length of the beam were noticed at all the mode shapes. For relatively thin beams, a modified Timoshenko beam theory, which takes care of the above-mentioned electric potential distribution, is suggested, and its detailed comparison with the present work will be the subject of a future publication.

For nonlinear modeling, the electric enthalpy term was extended to include the cubic nonlinearities. Similarly, the constitutive relations were extended to include the dissipative and nondissipative cubic order terms. During modeling of the longitudinal vibration of transversally polarized piezoceramics in Refs. [6,32], it was observed that quadratic terms did not appear in the first-order approximation in the perturbation solution. To force the quadratic term to appear in the first-order approximation, they had to be assumed to be of a higher order than cubic, which

was against the experimental observation. However, they also observed that the cubic terms alone can give rise to the nonlinear behavior, as observed in the experimental results. Hence, in the present case the nonlinear constitutive terms were restricted to only the cubic terms. Based on the observations in Ref. [9] of free piezoceramic vibrations using the d_{15} effect, only the constitutive relations for T_5 and D_1 were extended to include the cubic-order terms.

Hamilton's principle was used to obtain the nonlinear equation of motion of the piezoceramic beam. Linear eigenfunctions were used as shape functions in the Ritz method to discretize the nonlinear equation of motion. Perturbation methods were used to solve approximately the nonlinear equation of motion. A good coincidence between the experimental and the theoretical results was observed for the identified parameters of the piezoceramic. It was observed that, using different small subsets of parameters, it was possible to match the theoretical response curves with the experimental results.

The nonlinear effects observed in the present paper are not negligible. Therefore, they should be taken into account in the design of the devices, such as ultrasonic motors and torsional actuators, utilizing the d_{15} effect near resonance frequency excitation.

Appendix A. Polynomial functions

The starting functions for U and W are

$$\beta_0(x_1) = \delta_0(x_1) = \text{constant}, \quad \gamma_0(x_3) = \zeta_0(x_3) = \text{constant} \times (x_3 + l/2), \tag{A.1}$$

while the starting functions for ϕ satisfying the electric boundary conditions are

$$\theta_0(x_1) = \text{constant} \times (1 - 4x_1^2/h^2), \quad \phi_0(x_3) = \text{constant}. \tag{A.2}$$

The higher-order functions are obtained using the Gram–Schmidt process [26] as follows:

$$\beta_1(x_1) = (x_1 - Q_1)\beta_0(x_1), \quad \beta_i(x_1) = (x_1 - Q_i)\beta_{i-1}(x_1) - R_i\beta_{i-2}(x_1) \tag{A.3}$$

and

$$Q_i = \frac{\int_{-h/2}^{h/2} x_1\sigma(x_1)\beta_{i-1}^2(x_1)\,\mathrm{d}x_1}{\int_{-h/2}^{h/2} \sigma(x_1)\beta_{i-1}^2(x_1)\,\mathrm{d}x_1}, \tag{A.4}$$

$$R_i = \frac{\int_{-h/2}^{h/2} x_1\sigma(x_1)\beta_{i-1}(x_1)\beta_{i-2}(x_1)\,\mathrm{d}x_1}{\int_{-h/2}^{h/2} \sigma(x_1)\beta_{i-2}^2(x_1)\,\mathrm{d}x_1}. \tag{A.5}$$

$\sigma(x_1)$ is the weighting function, and unity in the present case. In case of $\gamma_j(x_3), \zeta_n(x_3), \phi_s(x_3)$ the interval is from $-l/2$ to $l/2$. MATLAB® 6.5 Symbolic toolbox is used in the present work to obtain the higher-order polynomials.

Appendix B. Expression for maximum kinetic and potential energies

Using Eqs. (20) and (21), the maximum kinetic energy can be written as

$$T_{\max} = \tfrac{1}{2}\rho b\omega^2 \int_A (\{\mathrm{A}\}^{\mathrm{T}}\{G_1\}\{G_1\}^{\mathrm{T}}\{\mathrm{A}\} + \{\mathrm{B}\}^{\mathrm{T}}\{G_2\}\{G_2\}^{\mathrm{T}}\{\mathrm{B}\})\,\mathrm{d}A \tag{B.1}$$

and using Eqs. (19), (21) and (22), the maximum potential energy can be written as

$$\begin{aligned} H_{\max} = \tfrac{1}{2}b \int_A \big(&\overline{c}_{11}\{\mathrm{A}\}^{\mathrm{T}}\{G_{1,1}\}\{G_{1,1}\}^{\mathrm{T}}\{\mathrm{A}\} + \overline{c}_{33}\{\mathrm{B}\}^{\mathrm{T}}\{G_{2,3}\}\{G_{2,3}\}^{\mathrm{T}}\{\mathrm{B}\} + c_{44}^{E}\{\mathrm{A}\}^{\mathrm{T}}\{G_{1,3}\}\{G_{1,3}\}^{\mathrm{T}}\{\mathrm{A}\} \\ &+ c_{44}^{E}\{\mathrm{B}\}^{\mathrm{T}}\{G_{2,1}\}\{G_{2,1}\}^{\mathrm{T}}\{\mathrm{B}\} + 2\overline{c}_{13}\{\mathrm{A}\}^{\mathrm{T}}\{G_{1,1}\}\{G_{2,3}\}^{\mathrm{T}}\{\mathrm{B}\} + 2\overline{e}_{31}\{\mathrm{A}\}^{\mathrm{T}}\{G_{1,1}\}\{G_{3,3}\}^{\mathrm{T}}\{\mathrm{C}\} \\ &+ 2\overline{e}_{33}\{\mathrm{B}\}^{\mathrm{T}}\{G_{2,3}\}\{G_{3,3}\}^{\mathrm{T}}\{\mathrm{C}\} + 2e_{15}\{\mathrm{A}\}^{\mathrm{T}}\{G_{1,3}\}\{G_{3,1}\}^{\mathrm{T}}\{\mathrm{C}\} + 2e_{15}\{\mathrm{B}\}^{\mathrm{T}}\{G_{2,1}\}\{G_{3,1}\}^{\mathrm{T}}\{\mathrm{C}\} \\ &+ 2c_{44}^{E}\{\mathrm{A}\}^{\mathrm{T}}\{G_{1,3}\}\{G_{2,1}\}^{\mathrm{T}}\{\mathrm{B}\} - \varepsilon_{11}^{S}\{\mathrm{C}\}^{\mathrm{T}}\{G_{3,1}\}\{G_{3,1}\}^{\mathrm{T}}\{\mathrm{C}\} - \overline{\varepsilon}_{33}\{\mathrm{C}\}^{\mathrm{T}}\{G_{3,3}\}\{G_{3,3}\}^{\mathrm{T}}\{\mathrm{C}\}\big)\,\mathrm{d}A. \end{aligned} \tag{B.2}$$

Appendix C. Elements of the matrices

$$[K_{\mathrm{mech}}] = \begin{bmatrix} \overline{c}_{11}\{G_{1,1}\}\{G_{1,1}\}^{\mathrm{T}} + c_{44}^{E}\{G_{1,3}\}\{G_{1,3}\}^{\mathrm{T}} & \overline{c}_{13}\{G_{1,1}\}\{G_{2,3}\}^{\mathrm{T}} + c_{44}^{E}\{G_{1,3}\}\{G_{2,1}\}^{\mathrm{T}} \\ \overline{c}_{13}\{G_{2,3}\}\{G_{1,1}\}^{\mathrm{T}} + c_{44}^{E}\{G_{2,1}\}\{G_{1,3}\}^{\mathrm{T}} & \overline{c}_{33}\{G_{2,3}\}\{G_{2,3}\}^{\mathrm{T}} + c_{44}^{E}\{G_{2,1}\}\{G_{2,1}\}^{\mathrm{T}} \end{bmatrix}, \tag{C.1}$$

$$[K_{\mathrm{piezo}}] = \begin{bmatrix} \overline{e}_{31}\{G_{1,1}\}\{G_{3,3}\}^{\mathrm{T}} + e_{15}\{G_{1,3}\}\{G_{3,1}\}^{\mathrm{T}} \\ \overline{e}_{33}\{G_{2,3}\}\{G_{3,3}\}^{\mathrm{T}} + e_{15}\{G_{2,1}\}\{G_{3,1}\}^{\mathrm{T}} \end{bmatrix}, \tag{C.2}$$

$$[K_{\mathrm{dielectric}}] = \left[-\varepsilon_{11}^{S}\{G_{3,1}\}\{G_{3,1}\}^{\mathrm{T}} - \overline{\varepsilon}_{33}\{G_{3,3}\}\{G_{3,3}\}^{\mathrm{T}}\right]. \tag{C.3}$$

References

[1] M. Kamlah, Ferroelectric and ferroelastic piezoceramics—modeling of electromechanical hysteresis phenomena, *Continuum Mechanics and Thermodynamics* 13 (2001) 219–268.

[2] H. Beige, G. Schmidt, Electromechanical resonances for investigating linear and nonlinear properties of dielectrics, *Ferroelectrics* 41 (1982) 39–49.

[3] P. Drögmöller, G. Gerlach, Jump phenomena of current in PZT-vibrators due to non-linear damping of the surrounding media, *Journal of European Ceramic Society* 21 (2001) 1395–1398.

[4] W. Jiang, W. Cao, Nonlinear properties of lead zirconate–titanate piezoceramics, *Journal of Applied Physics* 88 (11) (2000) 6684–6689.

[5] V. Mueller, Q.M. Zhang, Shear response of lead zirconate titanate piezoceramics, *Journal of Applied Physics* 83 (7) (1998) 3754–3761.

[6] S.K. Parashar, U. von Wagner, Nonlinear longitudinal vibrations of transversally polarised piezoceramics: experiments and modeling, *Nonlinear Dynamics* 37 (2004) 51–73.

[7] U. von Wagner, S.K. Parashar, Nonlinear longitudinal vibrations of transversally polarised piezoceramics, *Proceedings of the Fourth International Symposium of Continuous Systems*, Keswick, UK, 2003, pp. 51–53.

[8] U. von Wagner, Non-linear longitudinal vibrations of piezoceramics excited by weak electric fields, *International Journal of Non-Linear Mechanics* 38 (4) (2003) 565–574.
[9] S.K. Parashar, A. DasGupta, U. von Wagner, P. Hagedorn, Nonlinear shear vibrations of piezoceramic actuators, *International Journal of Non-Linear Mechanics* 40 (4) (2005) 429–443.
[10] S.K. Parashar, A. DasGupta, P. Hagedorn, Investigation of nonlinear shear induced flexural vibrations of piezoceramic actuators, *Proceedings of the SPIE Smart Structures and Materials 2004: Modeling, Signal Processing and Control, Vol. 5383, San Diego, CA*, 2004, pp. 71–81.
[11] C.T. Sun, X.D. Zhang, Use of thickness-shear mode in adaptive sandwich structures, *Smart Materials and Structures* 4 (1995) 202–206.
[12] X.D. Zhang, C.T. Sun, Formulation of an adaptive sandwich beam, *Smart Materials and Structures* 5 (1996) 814–823.
[13] X.D. Zhang, C.T. Sun, Analysis of a sandwich plate containing a piezoelectric core, *Smart Materials and Structures* 8 (1999) 31–40.
[14] A. Benjeddou, M.A. Trindade, R. Ohayon, A unified beam finite element model for extension and shear piezoelectric actuation mechanisms, *Journal of Intelligent Material Systems and Structures* 8 (1997) 1012–1025.
[15] M.A. Trindade, A. Benjeddou, R. Ohayon, Parametric analysis of the vibration control of sandwich beams through shear-based piezoelectric actuation, *Journal of Intelligent Material Systems and Structures* 10 (1999) 377–385.
[16] O.J. Aldraihem, A.A. Khdeir, Smart beams with extension and thickness-shear piezoelectric actuators, *Smart Materials and Structures* 9 (2000) 1–9.
[17] S.S. Vel, R.C. Batra, Exact solution for rectangular sandwich plates with embedded piezoelectric shear actuators, *AIAA Journal* 39 (2001) 1363–1373.
[18] S.S. Vel, R.C. Batra, Exact solution for the cylindrical bending of laminated plates with embedded piezoelectric shear actuators, *Smart Materials and Structures* 10 (2001) 240–251.
[19] A.E. Glazounov, Q.M. Zhang, C. Kim, Torsional actuator and stepper motor based on piezoelectric d_{15} shear response, *Journal of Intelligent Material Systems and Structures* 11 (2000) 456–468.
[20] A.E. Glazounov, S. Wang, Q.M. Zhang, C. Kim, Piezoelectric stepper motor with direct coupling mechanism to achieve high efficiency and precise control of motion, *IEEE Transactions on Ultrasonics, Ferroelectrics, and Frequency Control* 47 (4) (2000) 1059–1067.
[21] J. Kim, B. Kang, Performance test and improvement of piezoelectric torsional actuators, *Smart Materials and Structures* 10 (2001) 750–757.
[22] S. Dong, H.W. Kim, M.T. Strauss, K. Uchino, D. Viehland, A piezoelectric shear-shear mode ultrasonic motor, *Proceedings of the Eighth International Conference on New Actuators*, Bremen, Germany, 2002, pp. 126–129.
[23] H.F. Tiersten, *Linear Piezoelectric Plate Vibrations*, Plenum Press, New York, 1969.
[24] IEEE Std., *IEEE Standards on Piezoelectricity*, The Institute of Electrical and Electronics Engineers, New York, 1987.
[25] W.P. Mason, *Piezoelectric Crystals and Their Application to Ultrasonics*, Van Nostrand, New York, 1950.
[26] R.B. Bhat, Natural frequencies of rectangular plates using characteristic orthogonal polynomials in Rayleigh–Ritz method, *Journal of Sound and Vibration* 102 (1985) 493–499.
[27] S.M. Dickinson, A. Di Blasio, On the use of orthogonal polynomials in the Rayleigh–Ritz method for the study of the flexural vibration and buckling of isotropic and orthotropic rectangular plates, *Journal of Sound and Vibration* 108 (1) (1986) 51–62.
[28] G.M. Oosterhout, P.J.M. Van Der Hoogt, R.M.E.J. Spiering, Accurate calculation methods for natural frequencies of plates with special attention to the higher modes, *Journal of Sound and Vibration* 183 (1) (1995) 33–47.
[29] A. Graham, *Kronecker Products and Matrix Calculus with Applications*, Halsted Press, Wiley, New York, 1981.
[30] Q. Wang, S.T. Quek, Flexural vibration analysis of sandwich beam coupled with piezoelectric actuator, *Smart Materials and Structures* 9 (2000) 103–109.
[31] X. Liu, Q. Wang, S.T. Quek, Analytical solution for free vibration of piezoelectric coupled moderately thick circular plates, *International Journal of Solids and Structures* 39 (2002) 2129–2151.

[32] U. von Wagner, Nichtlineare Effekte bei Piezokeramiken unter schwachem elektrischem Feld: Experimentelle Untersuchung und Modellbildung, Habilitation Thesis, Technische Universität Darmstadt, GCA-Verlag, Herdecke, 2003.
[33] G.A. Maugin, *Nonlinear Electromagnetical Effects and Their Application*, World Scientific, Singapore, 1985.
[34] T. Ikeda, *Fundamentals of Piezoelectricity*, Oxford University Press, Oxford, 1990.
[35] U. von Wagner, P. Hagedorn, Piezo-beam system subjected to weak electric field: experiments and modelling of non-linearities, *Journal of Sound and Vibration* 256 (5) (2002) 861–872.
[36] U. von Wagner, P. Hagedorn, Nonlinear effects of piezoceramics excited by weak electric fields, *Nonlinear Dynamics* 31 (2003) 133–149.
[37] A.H. Nayfeh, D. Mook, *Nonlinear Oscillations*, Wiley, New York, 1979.